ACS Photonics

Article

pubs.acs.org/journal/apchd5

# Angle-Dependent Quality Factor of Mie Resonances in Silicon-Colloid-Based Microcavities

Lei Shi,*[,†,‡,§] Roberto Fenollosa,[†,§] T. Umut Tuzer,[†,§] and Francisco Meseguer[†,§]

[†]Centro de Tecnologias Fisicas, Unidad Asociada ICMM/CSIC-UPV, Universidad Politecnica de Valencia Avenida Los Naranjos s/n, Valencia, 46022, Spain

[‡]Department of Physics, Key Laboratory of Micro & Nano Photonic Structures (MOE) and Key Laboratory of Surface Physics, Fudan University, Shanghai 200433, People's Republic of China

[§]Instituto de Ciencia de Materiales de Madrid CSIC, Madrid, 28049, Spain

*Supporting Information*

**ABSTRACT:** Semiconductor photonic microcavities are currently very important elements in the field of photonics. We here report the light-trapping ability of 3D silicon spherical micrometer-sized photonic cavities, which are fabricated via simple chemical methods, as well as the results of quality factor measurements. We show, through both experiments and theoretical modeling, that the observed quality factor of the modes of a spherical silicon microcavity located on a dielectric substrate can be easily tuned by changing only the incident angle of the light. This special angle-dependent property could be used to design high-efficiency angle-resolved photodetectors and micrometer-sized optoelectronic power sources.

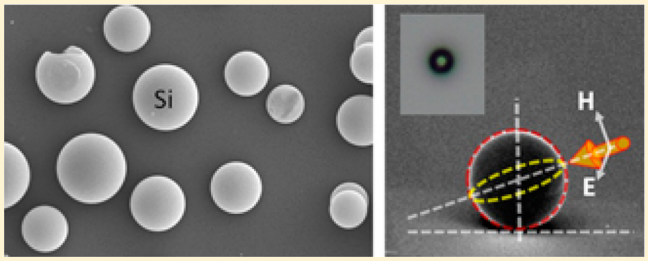


**KEYWORDS:** *semiconductor photonic cavity, silicon colloids, quality factor, Mie resonance*

Semiconductor photonic cavities (SPCs) are one of the most important optical components used in modern technology. The ability of SPCs to confine light in a small volume[1] and the enormous optoelectronic applications developed thus far[2] have focused on SPCs as key elements for the technological developments expected in the near future. Numerous types of SPCs, such as one- or two-dimensional (2D) photonic crystal cavities[3,4] and microdisk cavities,[5,6] have been reported. These SPCs can trap light very efficiently and can be easily integrated into photonic microcircuitry. Three-dimensional (3D) SPCs such as spherical cavities have been researched much less extensively because of the intrinsic difficulties related to their fabrication. Recently, some of us have reported on silicon spherical nano-[7] and microcavities[8] fabricated using chemical vapor deposition (CVD) techniques. The studies performed thus far have been focused on the cavity performance of these silicon-colloid-based SPCs[7−9] as well as on their applications in different types of devices.[10−12] Normally, as opposed to the 2D SPCs where light is coupled into the cavity via the near field, such as the evanescent field of the waveguide, silicon-colloid-based 3D SPCs are positioned on a certain substrate such that the light couples into the cavity from the far field. Because the resonance plane of the 3D cavity touches the substrate at only one point, the influence of the substrate appears to be negligible, especially in the cases of substrates with low refractive indexes. The Mie theory of isolated microcavities can therefore account for experimental results. This hypothesis, however, has never been proven.

With theoretical and experimental evidence, we show how the substrate substantially influences the optical properties of silicon-colloid-based SPCs. We analyze the influence of the substrate on the quality factor ($Q$) of the resonant modes, which is a key parameter for assessing the quality performance of a photonic cavity. A higher value of $Q$ indicates a longer lifetime of the photons trapped inside the cavity and a narrower resonance. However, a higher $Q$ value does not always indicate better device performance. High $Q$ values[1,3−5] are necessary in some research fields such as nonlinear optics and quantum information.[13−15] In other applications, such as those concerning luminescence emission enhancement of a lucent species inside a cavity,[16,17] moderate $Q$-factors are necessary. In the case of cavity-based photovoltaic devices, an optimum value of $Q$ exists that depends on the absorption coefficient for achieving the maximum absorption efficiency.[2,18−20] Therefore, investigations of the environmental factors that influence the $Q$-factor of a cavity are important and can provide new ideas about tuning this parameter in a controlled manner. In this paper, we demonstrate how the observed $Q$-factor of a silicon-colloid-based SPC can be easily modified by changing the direction of the incident light. This angle-dependent property could lead to optimization of $Q$ values for devices such as high-efficiency angle-resolved photodetectors and micrometer-sized optoelectronic power sources.[21,22]

**Received:** November 22, 2013
**Published:** April 11, 2014

  

We fabricated silicon-colloid-based SPCs via a chemical vapor deposition method using disilane ($Si_2H_6$) as a precursor gas, as described elsewhere (see also the Methods section).[8] This processing method is quick, inexpensive, and compatible with the industrial silicon CVD fabrication process; the silicon spherical cavities have a very small volume (their diameters are approximately 2−3 $\mu$m, as shown here), and the silicon spherical cavities exhibit a high optical performance (shown below). Figure 1a shows an optical microscopy image of a typical silicon spherical SPC. A scanning electron microscopy (SEM) image of the cavity is also shown in the figure inset. Additional SEM images of the fabricated silicon spherical SPC are provided in the Supporting Information (Figure S1). In general, the fabricated silicon spherical SPCs have a quite perfect spherical shape, although some have defects. Through micromanipulation techniques, we selected and positioned defect-free fabricated SPCs on a glass substrate. We performed angle-resolved optical transmission experiments on single particles using a custom-made confocal microscope (details shown in the Methods section) attached to a spectrometer with an InGaAs detector.

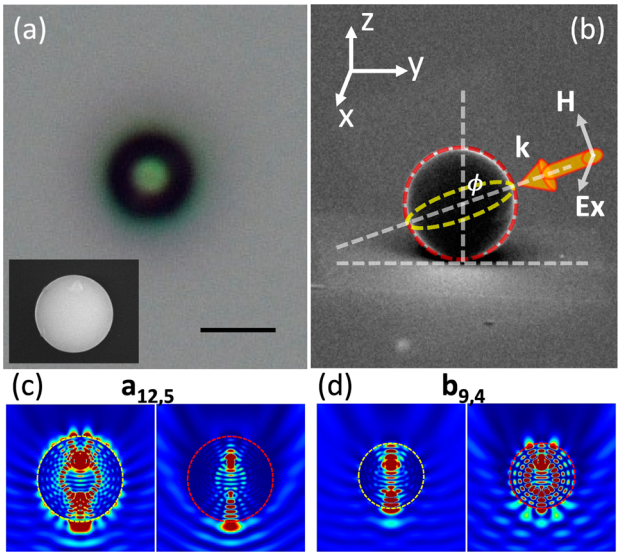


**Figure 1.** (a) Optical and SEM (inset) images of a typical silicon spherical microcavity. The bar is 3 $\mu$m. (b) Schematic view of the microcavity on a glass substrate. The orange arrow indicates the $k$ vector of the incident light; $\phi$ is the angle between the $k$ wavevector and the $z$ direction. The light is polarized linearly with the electric field, Ex, pointing in the $x$ direction. The light defines two planes: one parallel (dashed yellow line) and the other perpendicular (dashed red line) to Ex, where "a" and "b" modes occur, respectively. (c, d) Electric field distribution of $a_{12,5}$ (c) and $b_{9,4}$ (d) Mie modes in the two perpendicular planes indicated in (b). These modes are associated with the measured transmission dips at approximately 1.065 $\mu$m for a 3.31 $\mu$m SPC (Figure 2a) and 1.16 $\mu$m for a 2.546 $\mu$m SPC (Figure 2b).

Before showing the experimental and theoretical results of the angle-resolved optical properties, we first discuss how the observed $Q$-factor of different optical modes of a spherical silicon microcavity located on a substrate depends on the direction of the incident light. An isolated photonic cavity with a spherical shape should have isotropic optical properties, which are well described by the Mie theory, where all the Mie modes can be separated into two groups. The modes of the first group, labeled as the "a" group, resonate in a plane parallel to the electric component of the incident light. The modes of the second group, labeled as the "b" group, resonate in a plane perpendicular to the electric component of the incident light.[23] Whenever the spherical cavity is placed on a certain dielectric substrate, the isotropy of the Mie modes is destroyed, and the $Q$-factors of those degenerated or broken modes observed from the experiments could be strongly dependent on the incident angle of the light. This dependence occurs especially for those modes whose resonant plane intersects with the substrate. Figure 1b shows a schematic view of an s-wave polarized light impinging on a spherical silicon SPC located on a substrate at a certain incident angle $\phi$ as well as both resonance planes corresponding to the "a" (yellow dashed line) and the "b" (red dashed line) modes. The separate influence of the light incident angle on the observed $Q$-factors of the "a" and "b" modes is then easily understood. Whereas the resonance plane of the "b" modes (red dashed line) always intersects at 90 deg with the substrate (irrespective of the angle $\phi$), the resonant plane of the "a" modes (yellow dashed line) intersects at 90 deg with the substrate only for $\phi$ equal to zero. The "b" modes are therefore expected to be highly influenced by the presence of the substrate, independent of the incidence angle $\phi$ where the Mie resonances show smaller $Q$-factors than in the ideal case. The resonances of the "a" modes depend critically on the incident angle of light, and the interaction with the substrate decreases as $\phi$ increases. In any case, the influence of the substrate for each mode will depend on its particular electromagnetic field distribution and its extension in the mode volume. For example, Figure 1c and d show the electric field intensity distribution of modes $a_{12,5}$ and $b_{9,4}$, respectively, in the two perpendicular planes defined by the dashed yellow (left panels) and dashed red (right panels) lines. These two modes correspond to the measured transmission dips of approximately 1.065 $\mu$m for a 3.31 $\mu$m SPC (Figure 2a) and 1.16 $\mu$m for a 2.546 $\mu$m SPC (Figure 2b). Both modes are distributed in all of the spherical volume. However, for the $a_{12,5}$ mode, the electric field is much more concentrated in the yellow dashed line plane, which should be the resonant plane for all of the "a" modes. In the case of the $b_{9,4}$ mode, the electric field is more concentrated in the red dashed line plane, which should be the resonant plane for all of the "b" modes. In the case of p-wave incidence, similar analyses can easily be repeated, with opposite results; that is, in this case, the observed $Q$-factor of the "b" modes is expected to vary with $\phi$. In summary, we expect that the experimentally observed $Q$-factor of both types of modes can be easily tuned by changing the $k$-vector of the incident light and by choosing the appropriate polarization. For nonpolarized light, we obviously expect the observed $Q$-factor of all of the modes to increase as the angle of the incident light increases. The scattering with nonpolarized light occurs in numerous applications, including micro- or nano-optoelectronic power sources and photondetectors, and the scattering is studied here in detail.

Figure 2 shows the optical transmission properties of spherical SPCs on a glass substrate for three different diameter values: 3.310 $\mu$m (Figure 2a), 2.546 $\mu$m (Figure 2b), and 2.348 $\mu$m (Figure 2c). These values are the result of a fitting process, which will be explained below. The transmission dips in each spectrum correspond to Mie resonances. Smaller cavities result in fewer Mie modes that can be supported in a finite range of measurement; consequently, fewer transmission dips are observed. For all of the cavities, we shone nonpolarized light at different incident angles. The bottom black lines correspond


dx.doi.org/10.1021/ph400134t | ACS Photonics 2014, 1, 408−412

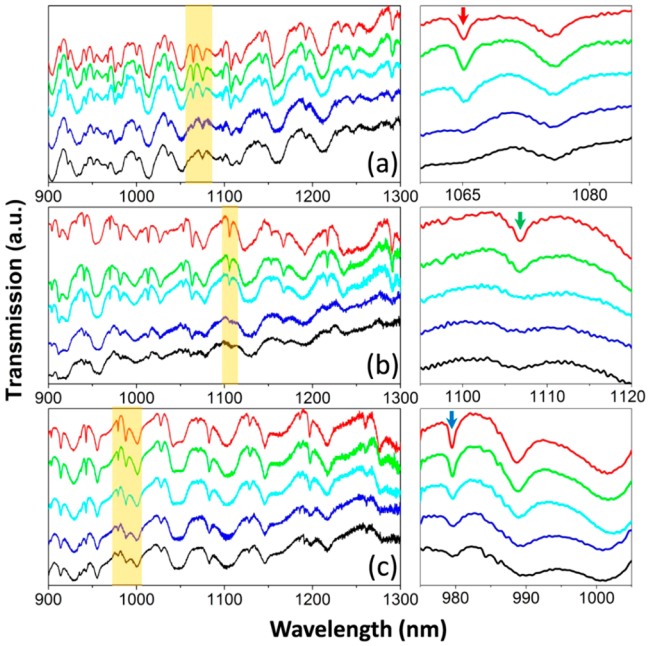


**Figure 2.** Optical transmission properties of silicon spherical cavities located on a glass substrate for three different diameter values: 3.310 $\mu$m (a), 2.546 $\mu$m (b), and 2.348 $\mu$m (c). The areas highlighted by orange in the left panels are magnified in the right panels. Black, blue, light-blue, green, and red curves correspond to light incident angles of 0° or normal, 20°, 40°, 60°, and 70°, respectively. To show all the spectra clearly, they have been shifted vertically to each other. The red, green, and blue arrows in the right panels indicate the $a_{12,5}$, $b_{9,4}$, and $b_{10,4}$ Mie resonances, respectively; the $Q$ variation of these resonances is analyzed in Figure 4.

to the normal incident case ($\phi$ = 0). The blue, light blue, green, and red lines correspond to 20, 40, 60, and 70 degrees of incidence, respectively. For the $\phi$ = 0 case, all of the transmission dips of all the cavities were broad, which indicates low $Q$ values of the Mie modes. When the incident angle was gradually increased, most of the transmission dips became sharper and even new transmission dips appeared. To show these results clearly, we magnified the areas marked by an orange band in the spectra in the right panels of Figure 2. The positions of three modes—$a_{12,5}$, $b_{9,4}$, and $b_{10,4}$—are indicated in these panels by red, green, and blue arrows, respectively; the variation of $Q$ as a function of the incident angle was studied in more detail, as described in the discussion of Figure 4.

To better understand the experimental results, we performed theoretical simulations of the scattering efficiency of single spherical silicon SPCs on a glass substrate at different values of the incidence angle using the null-field method with discrete sources (details are provided in the Methods section). In the calculations, we assumed a refractive index dispersion similar to that of silicon grown by plasma-enhanced chemical vapor deposition[24] (see Methods). This assumption allowed us to fit the experimental spectra to the theoretical simulations over the entire experimental measurement range by using the sphere diameter as the only fitting parameter. The refractive index of the glass was considered to have a constant value of 1.45. Figure 3 shows the calculated scattering efficiency of the silicon SPC with a diameter of 3.31 $\mu$m deposited on a glass substrate. Both s- and p-polarized light were used in the simulations. To mimic the experimental results, we calculated the mean value of the scattering efficiency contribution from the s- and p-polarizations. The different color spectra shown in the figure from the bottom (black spectrum) to the top (red spectrum) correspond to different angles of incidence, specifically, $\phi$ = 0°, 20°, 40°, 60°, and 70°. The corresponding experimental transmission spectra (see Figure 2a) are also shown for each angle (purple curves), revealing a reasonably good agreement between theory and experiment. The resonances obtained in experimental results appear here as peaks instead of dips because the transmission scales have been inverted. Similar to the experiments, the calculated spectrum for normal incidence shows broad resonances. High $Q$ value (narrow) peaks are also missing. When the incident angle of the light increases, the peaks become sharper and their $Q$ value increases. In the top panel of Figure 3, the calculated spectrum of a free-standing

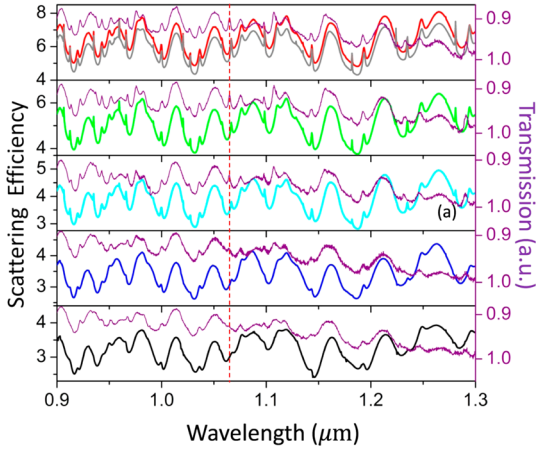


**Figure 3.** Theoretical simulations of light scattering on a 3.310 $\mu$m diameter silicon spherical cavity on a glass substrate. (a) Spectra at light incident angles, $\phi$, of 0°, 20°, 40°, 60°, and 70° are shown by black, blue, light blue, green, and red curves, respectively, in different panels. For comparison, the corresponding experimental spectrum is also included in each panel as a purple curve. The gray line in the top panel corresponds to the spectrum of the same cavity free-standing in air. This spectrum has been multiplied by 2.5 for better comparison. The vertical dashed line shows the position of the $a_{12,5}$ mode indicated by a red arrow in Figure 2

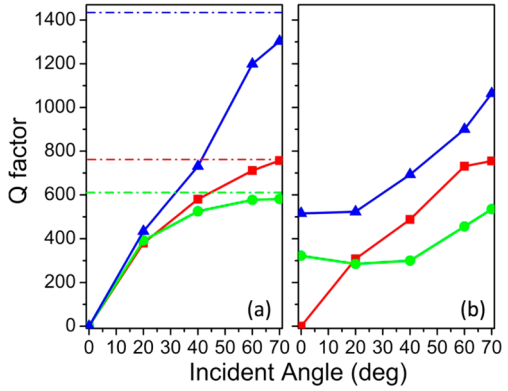


**Figure 4.** Quality ($Q$) factor value for the silicon colloid spherical microcavities on a glass substrate as a function of the incident angle of light. The symbols in (a) and (b) correspond to the $Q$ values taken from the theoretical simulations and from the experimental data, respectively. Red, green, and blue colors correspond to the $a_{12,5}$, $b_{9,4}$, and $b_{10,4}$ modes, respectively, which are indicated by arrows of the same color in Figure 2. The solid lines simply link the symbols. The dash-dotted lines indicate the "ideal" $Q$ values for the same cavities when they are free-standing in air.


dx.doi.org/10.1021/ph400134t | ACS Photonics 2014, 1, 408−412

silicon colloid SPC with the same diameter as that of the sample used to obtain the other spectra, i.e., 3.31 $\mu$m (gray line), is shown. The spectrum of the free-standing sphere is similar to that of the cavity on glass for the incident angle of $\phi$ = 70° (red curve), with some discrepancies in the high-$Q$ resonances because of the resolution of the spectra. The spectrum of the free-standing silicon colloid SPC was multiplied by 2.5 for better comparison with the other spectra. The contrast between the scattering efficiency and the resonance peaks increased substantially when the cavity was located on the glass substrate, as explained by the theory of the virtual mirror image beneath the surface of the substrate.[25,26] More calculation results for other sizes of silicon SPCs, showing a good agreement between theory and experiment, are plotted in the Supporting Information (Figure S2 and Figure S3). The calculated light scattering spectra of p- and s-waves for the "a" modes and the "b" modes for different-diameter silicon SPCs on a glass substrate are also shown in the Supporting Information. As previously discussed, this calculation confirms that, for the case of p-polarized incident light, the observed $Q$ value of the "b" modes is sensitive to the incidence angle of the light, whereas the "a" modes are not so sensitive. For the case of s-polarized incident light, the observed $Q$-factor of the "a" modes is more sensitive than that of the "b" modes.

Figure 4 shows the variation of the $Q$ values with the incident angle for the $a_{12,5}$ (red curves), the $b_{9,4}$ (green curves), and the $b_{10,4}$ (blue curves) modes. The $Q$ values are indicated by the same colored arrows in Figure 2 and by dashed lines in Figure 3, Figure S1, and Figure S2, respectively. Figure 4a shows the values taken from the theoretical simulations, and Figure 4b shows the values taken from the experimental data. The dot-dashed lines in Figure 4a indicate the $Q$ values for the cavities that are free-standing in air. We refer to them hereafter as "ideal $Q$ values". In general, as deduced from the theoretical simulations (Figure 4a), the observed $Q$ values of the three studied modes increase quickly as the incident angle increases from normal incidence, and the observed $Q$ values approach more slowly the ideal $Q$ values at higher angles, approximately 70°. The experimental $Q$ values (Figure 4b) were, in general, observed to be slightly smaller than the theoretical $Q$ values (see, for instance, the red curves for mode $a_{12,5}$). These results indicate that the fabricated cavities have a good quality in terms of their spherical geometry and the silicon homogeneity within the cavities. The main differences between experiment and theory appear at approximately the zero-degree incidence for the $b_{9,4}$ and $b_{10,4}$ modes. We attribute these discrepancies to the fact that the incident light was shone on the sample after passing through an objective with a certain numerical aperture, thus delivering light at incident angles different from zero. The reason that these discrepancies are observed for these modes and not for the other modes is attributed to their different electromagnetic field distributions. However, more research is necessary to clarify this fact.

In conclusion, we have shown that the $Q$ values of Mie resonances of a high-refractive-index spherical microcavity are strongly sensitive to the presence of substrates, even when the substrate has a low refractive index, such as the case of a glass substrate. The cavity−substrate interaction is angle-dependent and can be easily changed just by changing the incident angle of the light. Because of the relationship between the photon lifetime inside the cavity and the $Q$-factor of the cavity mode, the observed effect indicates that the lifetime of the photon trapped inside a 3D silicon colloid SPC depends strongly on the incident direction of the coupled photon. Our findings may find applications in angle-resolved photondetectors and micrometer-sized optoelectronic power sources.

## METHODS

The method used to obtain spherical silicon colloid microcavities was based on chemical vapor deposition techniques, where disilane gas ($Si_2H_6$) at high temperatures was decomposed into solid silicon and hydrogen gas by the following chemical reaction: $Si_2H_6(g) = 2Si(s) + 3H_2(g)$[8] (more details are provided in the Supporting Information). We used a quartz tube as a reactor and introduced disilane gas at a pressure of 30 kPa. The reactor was heated by a tubular oven to 420 °C. Silicon colloids were grown in the gas phase and fell onto the substrate, specifically, a silicon slab. The silicon colloids were detached from the silicon substrate and placed onto a clean glass substrate by micromanipulation with a glass tip. This glass substrate was placed onto a sample holder (able to rotate freely) of a custom-made confocal microscope, which allowed measurement of the spectra of the transmitted light. Nonpolarized light was shone from the glass substrate onto the silicon cavity. The objective used in the setup was 20× with a 0.4 numerical aperture. The light source was a tungsten lamp. Because of the low coherent properties of the emission from the thermal light source, the spot size (approximately 100 $\mu$m) of the incident light on the sample was much larger than the size of the measured silicon SPC (several $\mu$m). A plane-wave scenario was therefore reasonably assumed, which allowed us to perform the theoretical analysis on the basis of a plane-wave approximation.

In the theoretical simulations, we also assumed (as it appears in the experiment) that the incident light impinges from the glass substrate into the silicon cavity. We modified an existing code based on the null-field method with discrete sources[27] to calculate the scattering efficiency of the single silicon colloids on a glass substrate at different angles of incidence. In this method, the incident light and the scattering light can be expanded in terms of a series of vector spherical wave functions. The scattering problem can then be simplified as $S = \langle T \rangle I$, where $T$ is a transition matrix ($T$ matrix) that is only related to the scatterer and $S$ and $I$ are the expansion coefficients of the scattered and the incident fields, respectively. Here, *the null-field method is only one among many methods that can be used to compute the T matrix; furthermore, with discrete sources, the numerical method has greater numerical stability for the calculation of the T matrix. The plane waves were considered as external excitations. More details related to the methods and the program are provided by Doicu et al.*[27] For the nonpolarized light simulation, the results shown in this article were calculated on the basis of the formula $S_{nonpolar} = (S_{s\text{-}wave} + S_{p\text{-}wave})/2$. The refractive index, $n$, dispersion for silicon colloids was assumed to be given by the equation $n = A/\lambda^2 + B$,[24] where $\lambda$ is the wavelength of the light, $A = 1.686 \times 10^5$ nm$^2$, and $B = 3.097$.[24] This dispersion gives refractive index values lower than those of the bulk silicon; we attributed these lower refractive index values to the existence of some porosity.

## ASSOCIATED CONTENT

### Supporting Information

SEM images of the fabricated spherical silicon microcavities, scheme of the fabrication procedure and its detailed description, the theoretical scattering efficiency, and experimental transmission spectra of 2.546 and 2.348 $\mu$m diameter


dx.doi.org/10.1021/ph400134t | ACS Photonics 2014, 1, 408−412

silicon spherical cavities on a glass substrate are included in the Supporting Information. This material is available free of charge via the Internet at http://pubs.acs.org.

## AUTHOR INFORMATION


### Corresponding Author

*E-mail: shilei@upv.es.


### Notes

The authors declare no competing financial interest.

## ACKNOWLEDGMENTS

The authors acknowledge financial support from the following projects: MAT2012-35040, FIS2009-07812, Consolider 2007-0046 Nanolight, and the PROMETEO/2010/043. L.S. thanks the MICINN (Estancias de Profesores e Investigadores Extranjeros en Centros Españoles) fellowship program, the Starting Foundation from Fudan University, the NSFC, and the Shanghai Science and Technology Commission for their financial support.

## REFERENCES


(1) Vahala, K. J. Optical microcavities. *Nature* **2003**, *424*, 839−846.

(2) Unlu, M. S.; Strite, S. Resonant cavity enhanced photonic devices. *J. Appl. Phys.* **1995**, *78*, 607−639.

(3) Akahane, Y.; Asano, T.; Song, B. S.; Noda, S. High-Q photonic nanocavity in a two-dimensional photonic crystal. *Nature* **2003**, *425*, 944−947.

(4) Gerard, J. M.; Barrier, D.; Marzin, J. U.; Kuszelewicz, R.; Manin, L.; Costard, E.; Thierry-Mieg, V.; Rivera, T. Quantum boxes as active probes for photonic microstructures: the pillar microcavity case. *Appl. Phys. Lett.* **1996**, *69*, 449−451.

(5) Gayral, B.; Gerard, J. M.; Lemaitre, A.; Dupuis, C.; Manin, L.; Pelouard, J. L. High-Q wet-etched GaAs microdisks containing InAs quantum boxes. *Appl. Phys. Lett.* **1999**, *75*, 1908−1910.

(6) Boriskina, S. V. Theoretical prediction of a dramatic Q-factor enhancement and degeneracy removal of whispering gallery modes in symmetrical photonic molecules. *Opt. Lett.* **2006**, *31*, 338−340.

(7) Shi, L.; Tuzer, T. U.; Fenollosa, R.; Meseguer, F. A new dielectric metamaterial building block with a strong magnetic response in the sub-1.5-micrometer region: silicon colloid nanocavities. *Adv. Mater.* **2012**, *24*, 5934−5938.

(8) Fenollosa, R.; Meseguer, F.; Tymczenko, M. Silicon colloids: from microcavities to photonic sponges. *Adv. Mater.* **2008**, *20*, 95−98.

(9) Xifre-Perez, E.; Fenollosa, R.; Meseguer, F. Low order modes in microcavities based on silicon colloids. *Opt. Express* **2011**, *19*, 3455−3463.

(10) Xifre-Perez, E.; Domenech, J. D.; Fenollosa, R.; Munoz, P.; Capmany, J.; Meseguer, F. All silicon waveguide spherical microcavity coupler device. *Opt. Express* **2011**, *19*, 3185−3192.

(11) Shi, L.; Meseguer, F. Magnetic interaction in all silicon waveguide spherical coupler device. *Opt. Express* **2012**, *20*, 22616−22626.

(12) Shi, L.; Harris, J. T.; Fenollosa, R.; Rodriguez, I.; Lu, X.; Korgel, B. A.; Meseguer, F. Monodisperse silicon nanocavities and photonic crystals with magnetic response in the optical region. *Nat. Commun.* **2013**, *4*, 1904.

(13) Painter, O.; Lee, R. K.; Scherer, A.; Yariv, A.; O'Brien, J. D.; Dapkus, P. D.; Kim, I. Two-dimensional photonic band-gap defect mode laser. *Science* **1999**, *284*, 1819−1821.

(14) Tanaka, Y.; Upham, J.; Nagashima, T.; Sugiya, T.; Asano, T.; Noda, S. Dynamic control of the Q factor in a photonic crystal nanocavity. *Nat. Mater.* **2007**, *6*, 862−865.

(15) Tananbe, T.; Notomi, M.; Taniyama, H.; Kuramochi, E. Dynamic release of trapped light from an ultrahigh-Q nanocavity via adiabatic frequency tuning. *Phys. Rev. Lett.* **2009**, *102*, 043907.

(16) Haroche, S.; Kleppner, D. Cavity quantum electrodynamics. *Phys. Today* **1989**, *42*, 24−33.

(17) Chang, R. K.; Campillo, A. J., Eds. *Optical Processes in Microcavities*; World Scientific: Singapore, 1998.

(18) Chutinan, A.; John, S. Light trapping and absorption optimization in certain thin-film photonic crystal architectures. *Phys. Rev. A* **2008**, *78*, 023825.

(19) Callahan, D. M.; Munday, J. N.; Atwater, H. A. Solar cell light trapping beyond the ray optic limit. *Nano Lett.* **2012**, *12*, 214−218.

(20) Park, Y.; Drouard, E.; El Daif, O.; Letartre, X.; Viktorovitch, P.; Fave, A.; Kaminski, A.; Lemiti, M.; Seassal, C. Absorption enhancement using photonic crystals for silicon thin film solar cells. *Opt. Express* **2009**, *17*, 14312−14321.

(21) Chen, M.; Hu, L.; Xu, J.; Liao, M.; Wu, L.; Fang, X. ZnO hollow-sphere nanofilm-based high-preformance and low-cost photodetector. *Small* **2011**, *7*, 2449−2453.

(22) Tian, B.; Zheng, X.; Kempa, T. J.; Fang, Y.; Yu, N.; Yu, G.; Huang, J.; Lieber, C. M. Coaxial silicon nanowires as solar cells and nanoelectronic power sources. *Nature* **2007**, *449*, 885−889.

(23) Conwell, P. R.; Barber, P. W.; Rushforth, C. K. Resonant spectra of dielectric spheres. *J. Opt. Soc. Am. A* **1984**, *1*, 62−67.

(24) Badran, R. I.; Al-Hazmi, F. S.; Al-Heniti, S.; Al-Ghamdi, A. A.; Li, J.; Xiong, S. A study of optical properties of hydrogenated microcrystalline silicon films prepared by plasma enhanced chemical vapor deposition technique at different conditions of excited power and pressure. *Vacuum* **2009**, *83*, 1023−1030.

(25) Albooyeh, M.; Simovski, C. R. Huge local field enhancement in perfect plasmonic absorbers. *Opt. Express* **2012**, *20*, 21888−21895.

(26) Xifre-Perez, E.; Shi, L.; Tuzer, U.; Fenollosa, R.; Ramiro-Manzano, F.; Quidant, R.; Meseguer, F. Mirror-image-induced magnetic modes. *ACS Nano* **2013**, *7*, 664−668.

(27) Doicu, A.; Wriedt, T.; Eremin, Y. A. *Light Scattering by Systems of Particles*; Springer Verlag: Berlin, 2006.